SOLFEO

ESA Contract No 4000127610/19/I-NS

Product User Guide

NH_3 emissions

Date of issue: 24 August 2020

Author(s): Jieying Ding

Table of Contents

1 Introduction

1.1 Service description

Up-to-date and reliable emission inventories are essential for accurate air quality modelling and forecasting on various spatial scales. These inventories are also used by policy makers to evaluate the effectiveness of emission abatement measures, and to decide on future strategies. Here we use satellite observations of air constituents for deriving emissions. An advantage of these top-down emission estimates is the spatial and temporal consistency for all pollutants, a high temporal resolution, and the rapid availability.

Within the SOLFEO project emissions are derived for South America. The NH_3 emissions are derived with the DECSO inversion algorithm applied to IASI observations.

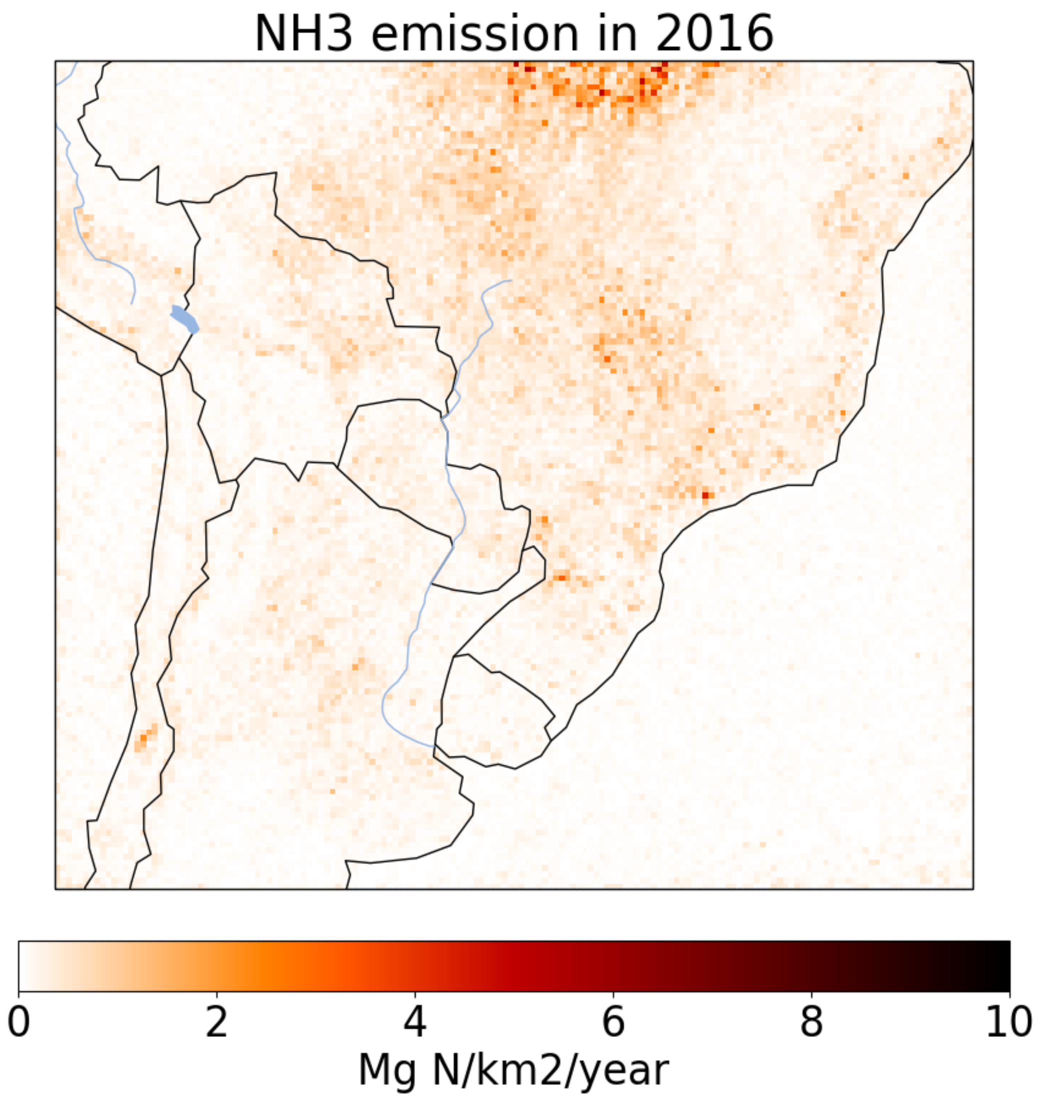

Figure 1. NH_3 emission for the year 2016 derived from the IASI observation from MetOp-A using the DECSO algorithm.

1.2 DECSO algorithm description

The DECSO algorithm [Mijling and Van der A, 2012] is specifically designed to use daily satellite observations of column concentrations for fast updates of emission estimates of short-lived atmospheric constituents on a mesoscopic scale (0.25°×0.25°). An extensive description of the algorithm can be found in the GlobEmission ATBD [2015].

We use the DECSO algorithm together with the regional chemistry-transport model CHIMERE on a 0.25° resolution, driven by operational meteorological forecast of the European Centre for Medium-Range Weather Forecasts (ECWMF). The model implementation is described in more detail by Ding et al. [2015]. We use NH_3 observations from the IASI instrument aboard the

MetOp-A satellite launched in October 2006. IASI is an infrared Fourier transform spectrometer, which circles in a polar Sun-synchronous orbit and operates in a nadir viewing mode with overpass times at 9:30 and 21:30 local solar time when it crosses over the Equator. IASI has an observational swath width of over 2000 km and a square field of view composed of four circular footprint of 12 km each at nadir, distorted to ellipse-shaped pixels off-nadir. We use the ANNI NH3 v2.1 reanalysis retrieval product from Van Damme et al. (2017). This product uses a neural network to link the hyperspectral range index (HRI) with a set of parameters, representing the atmospheric state, to derive the total NH_3 columns. The reanalysis dataset has small discontinuities by using the meteorological parameters from the ERA-Interim reanalysis and cloud coverage from EUMETSAT in near-real time. The dataset is downloaded from the Aeris data infrastructure (https://iasi.aeris-data.fr/nh3/). To use the data, we filter out the data lower than 4.8 x 10^{15} molecule/cm^2 due to the detection limit of IASI (2ppb, which is about 4.8 x 10^{15} molecule/cm^2) (Dammers et al., 2019).

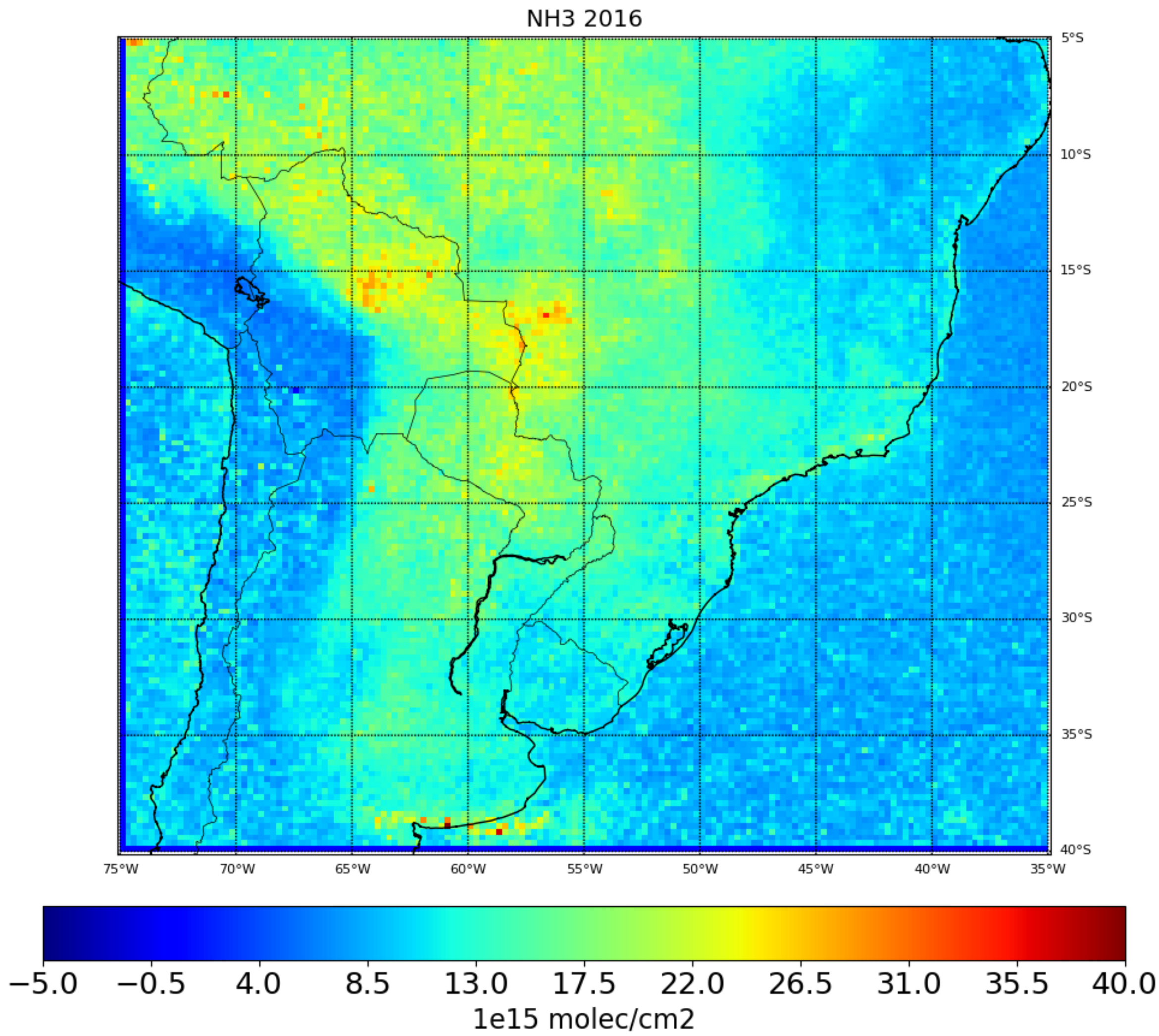

Figure 2 Averaged tropospheric NH_3 columns as observed by the IASI instrument aboard MetOp-A in 2016.

2 Product Specifications

2.1 Product description

Table 1. Output product description for emission inventory.

Product Type	Emission inventory. Air pollutants included: NH_3
Spatial Resolution	0.25 degrees
Temporal Range	January 2016 – December 2016
Temporal Resolution	Monthly averaged
Estimated accuracy	42%
Spatial Coverage	Domain: 40-5° S, 75-36° W
Format and Size	Format: netCDF Size: approximately 1.6 MB per file
Satellite data sources	IASI-MetOp-A

- The NH_3 (ammonia) emissions based on IASI for South America can be found at http://www.globemission.eu/region_samerica/datapage_nh3.php

2.2 Data structure

In table 2 the data structures of the SOLFEO NH_3 emission data is presented. In principle, the meta data description as well as the variables describe the data set in it full extend. The meta data include the data origin, comments, and domain description. As such the data products are compliant with GEOSS recommendations ensuring easy access to the data.

Table.2 Data structure for regional DECSO emission data in South America.

Attribute	Meta Data Description
X1: Description	Product description
X2: Author	name of creator
X3: Institution	name of institute
X4: Domain	Region with available data
X5: Year	Time period of emission inventory

X6: History	Date of creation
X7: grid_westb	west bound of regular grid
X8: grid_westb_unit	units of west bound of regular grid
X9: grid_eastb	east bound of regular grid
X10: grid_eastb_unit	units of east bound of regular grid
X11: grid_lon_res	longitudinal resolution of regular grid
X12: grid_lon_res_unit	units of longitudinal resolution of regular grid
X13: grid_dlon	longitudinal spacing of regular grid
X14: grid_dlon_unit	units of longitudinal spacing of regular grid
X15: grid_south	south bound of regular grid
X16: grid_southb_unit	units of south bound of regular grid
X17: grid_northb	north bound of regular grid
X18: grid_northb_unit	units of north bound of regular grid
X19: grid_lat_res	latitudinal resolution of regular grid
X20: grid_lat_res_unit	units of latitudinal resolution of regular grid
X21: grid_dlat	latitudinal spacing of regular grid
X22: grid_dlat_unit	units of latitudinal spacing of regular grid
Variable	**Description + unit**
V1: time	Time in days since the beginning of the year
V2: lat	cell latitudes in regular grid (cell centers) [degrees_north]
V3: lon	cell longitudes in regular grid (cell centers) [degrees_east]
V4: NH3	ammonia emission from source [10^{15} molecules/cm2/h]
V5: NH3_alt	ammonia emission from source [Gg N/cell/month]
V6: area	cell area in regular grid [km2]
Dimensions	**Definition**
time	Dimension of the time variable
lat	Dimension of the variable lat
lon	Dimension of the variable lon

3 Data quality and known issues

3.1 High altitudes

The CTM used in DECSO is modeling till a pressure level of about 500 hPa. For very high mountain ranges this can lead to too small model layers with unrealistic local model results. This can lead to unrealistic emissions over the Andes. Therefore, all data for grid cells with an average altitude above 3500 m has been removed. Figure 3 shows the altitude in the region of the emissions.

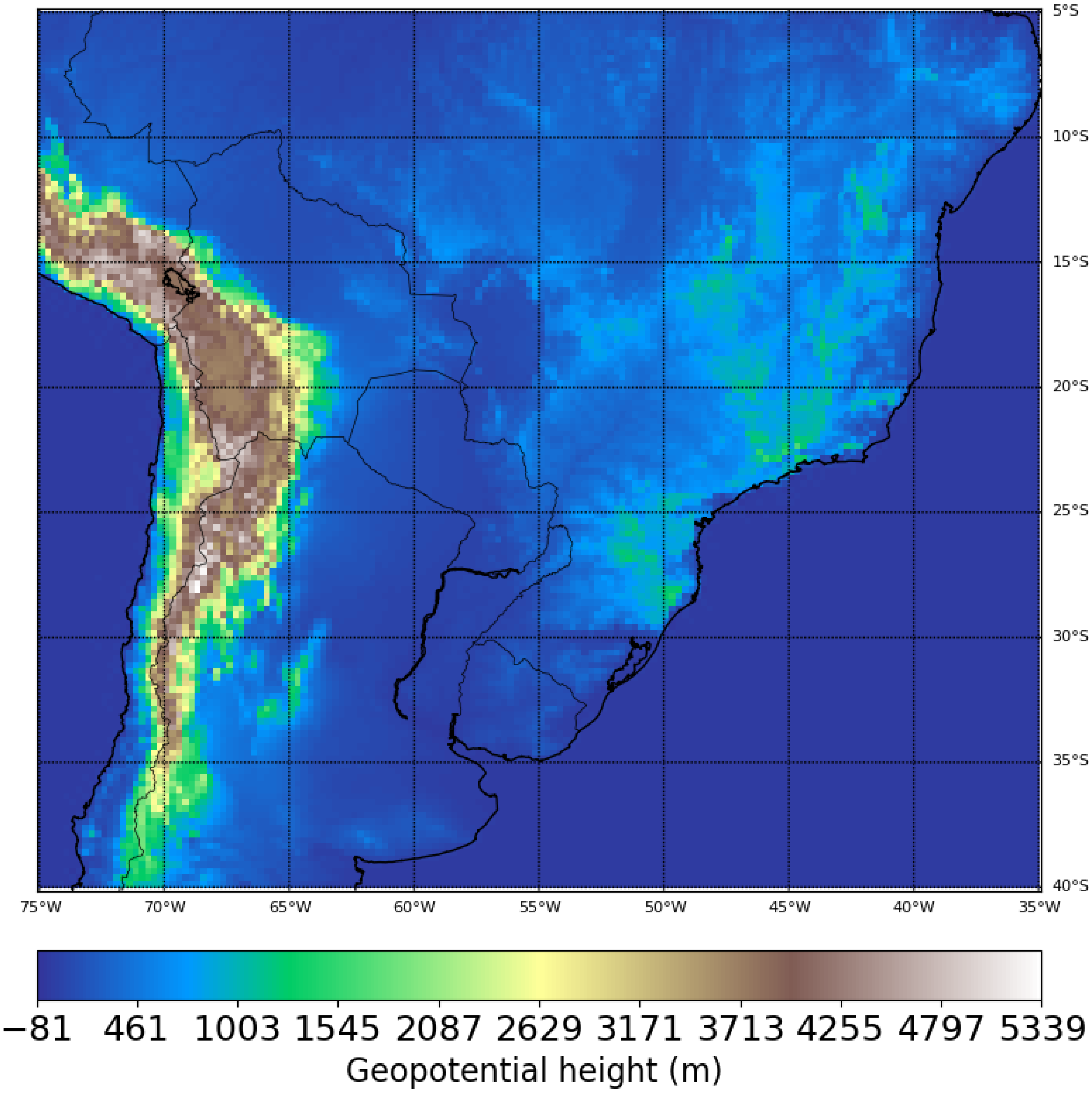

Figure 3 Geopotential height (m) in the region for which the emissions are provided.

3.2 IASI NH_3 validation

We use the NH_3 retrieval product of the version ANNI-NH3-v2.1R-I. The product combines the calculation of the dimensionless spectral index (HRI) with a neural network to calculate the total columns of NH_3. Dammers et al. (2019) and Van Damme et al. (2018) estimated NH_3 emissions from point sources using the same NH_3 retrieval product. The previous versions of the NH_3 product were validated by Dammers et al. (2016) and were found to have a low bias of about 40% and with better performance for the regions with high concentrations. Van Damme et al. (2017) stated that the ANNI NH3 v2.1 reanalysis retrieval product used for NH_3 emission estimates is self-consistent in time and is expected to be highly suitable to study long-term trends.

References:

Dammers, E., Palm, M., Van Damme, M., Vigouroux, C., Smale, D., Conway, S., Toon, G. C., Jones, N., Nussbaumer, E., Warneke, T., Petri, C., Clarisse, L., Clerbaux, C., Hermans, C., Lutsch, E., Strong, K., Hannigan, J. W., Nakajima, H., Morino, I., Herrera, B., Stremme, W., Grutter, M., Schaap, M., Wichink Kruit, R. J., Notholt, J., Coheur, P.-F., and Erisman, J. W.: An evaluation of IASI-NH3 with ground-based Fourier transform infrared spectroscopy measurements, Atmos. Chem. Phys., 16, 10351–10368, https://doi.org/10.5194/acp-16-10351-2016, 2016.

Dammers, E., McLinden, C. A., Griffin, D., Shephard, M. W., Van Der Graaf, S., Lutsch, E., et al.. (2019). NH_3 emissions from large point sources derived from CrIS and IASI satellite observations. Atmos. Chem. Phys., 19(19), 12261-12293. doi:10.5194/acp-19-12261-2019

Van Damme, M., Whitburn, S., Clarisse, L., Clerbaux, C., Hurtmans, D., and Coheur, P.-F.: Version 2 of the IASI NH_3 neural network retrieval algorithm: near-real-time and reanalysed datasets, Atmos. Meas. Tech., 10, 4905–4914, https://doi.org/10.5194/amt-10-4905-2017, 2017.

Van Damme, M., Clarisse, L., Whitburn, S., Hadji-Lazaro, J., Hurtmans, D., Clerbaux, C., & Coheur, P.-F. (2018). Industrial and agricultural ammonia point sources exposed. Nature, 564(7734), 99-103. doi:10.1038/s41586-018-0747-1

3.3 Comparison to HTAP

We use the HTAP (Hemispheric Transport Atmospheric Pollution) emission inventory version 2 in 2010 as our initial emissions to run the CTM. The spatial resolution of HTAP is $0.1^\circ \times 0.1^\circ$. HTAP uses nationally reported emissions combined with regional scientific inventories in the format of sector-specific grid maps. The database consists of a combination of gridded regional emission inventories such as the Model Inter-Comparison Study (MICS) for Asia, Environmental Protection Agency (EPA) for the US and Canada, and the Netherlands Organisation for Applied Scientific Research – Monitoring Atmospheric Composition and Climate (TNO-MACC) II database for Europe. The grid maps are complemented with EDGARv4.3 data for those regions where data are absent.

Figure 4 presents the monthly NH_3 emissions from HTAP in 2010. We see NH_3 emissions slightly increase or decrease with the same spatial distribution from month to month. Since the lifetime of NH_3 is very short, about a few hours, we expect the NH_3 emission distribution to be similar to the concentration. The monthly NH_3 column concentrations observed by IASI show different monthly distributions (Figure 5). We see a very strong seasonal variation on NH_3 column concentrations in the region. NH_3 column concentrations start to increase in the center of the domain in August. The high NH_3 concentrations are due to biomass burning emissions (van Damme et al., 2018). Figure 6 shows the NH_3 monthly emissions derived from satellite observations. We see a clear seasonal cycle from the figure.

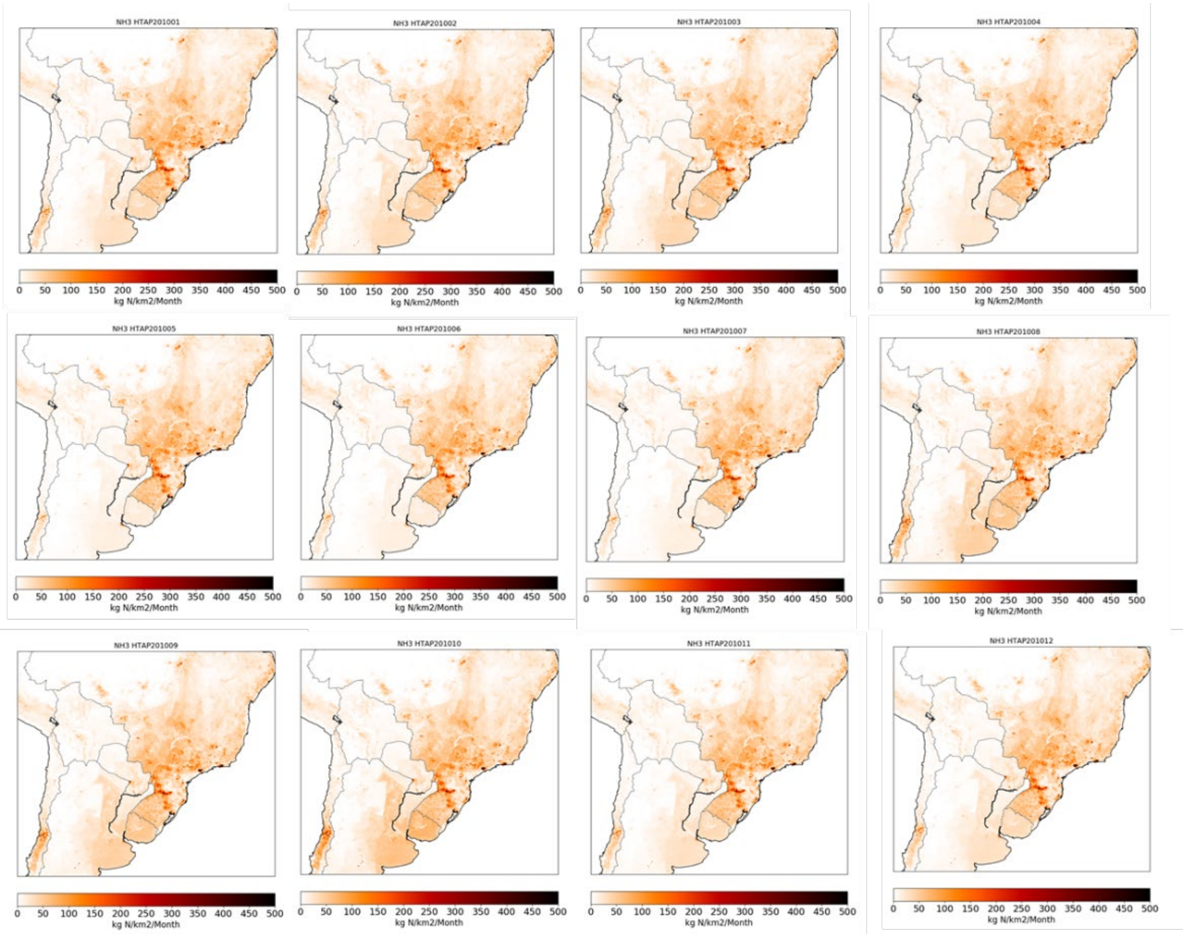

Figure 4. Monthly NH_3 emissions from HTAP 2010. Data are downloaded from https://edgar.jrc.ec.europa.eu/htap_v2/.

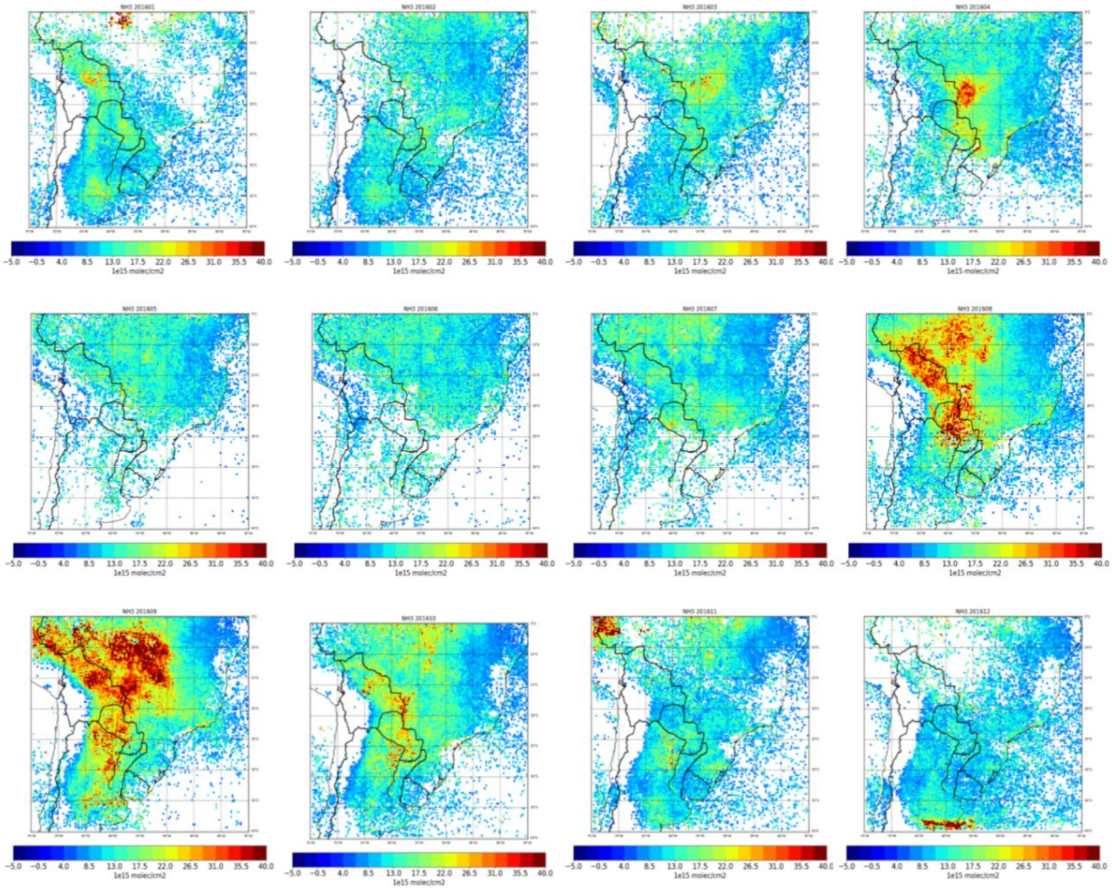

Figure 5. Monthly tropospheric NH_3 columns in 2016 as observed by the IASI instrument aboard MetOp-A.

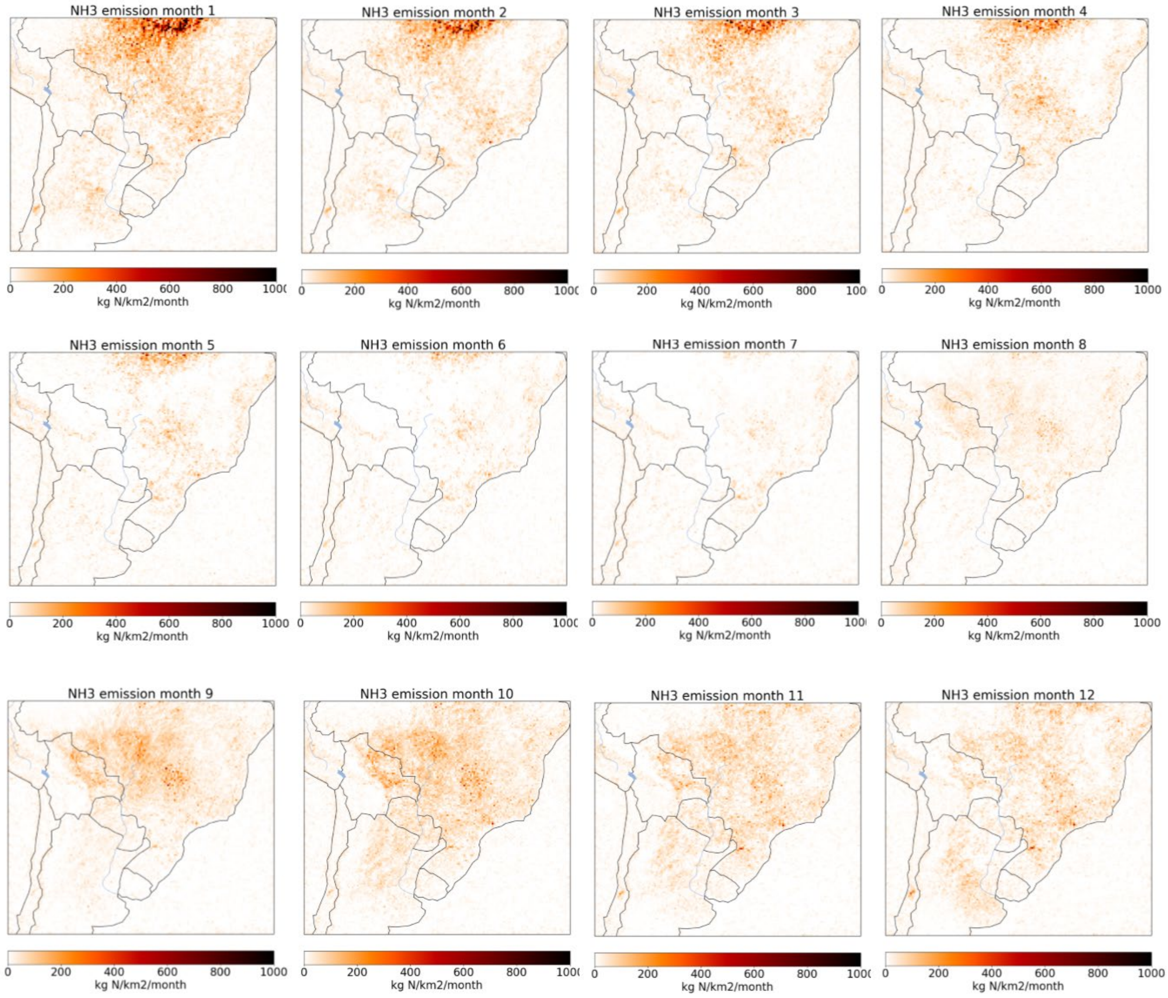

Figure 6. Monthly NH_3 emissions in 2016 derived with DECSO from IASI observations on MetOp-A.

3.4 Comparison to an Argentinian bottom-up inventory

We have compared the DECSO emissions to an Argentinian bottom-up emission inventory recently published in Puliafito et al.(2020). The bottom-up inventory contains emission for the year 2014 and 2016. We have resampled the 2016 NH_3 emissions to the same grid as DECSO for comparison. Figure 7 shows the comparison between the annual bottom-up and the annual averaged NH_3 emissions of DECSO. The bottom-up inventory of Argentina shows that NH_3 emissions are mainly distributed in the east part of Argentina (see figure 7). Two strong point sources are shown in the city area of Buenos Aires and Concepción del Uruguay. However, these two strong points are not seen from satellite observations and also not found in the point source emission study from Dammers et al. (2019) and van Damme et al. (2018). Figure 7 shows that NH_3 emissions estimated with DECSO from IASI on MetOp-A are mainly distributed over cropland and herbaceous areas (see the land use map of Figure 8).

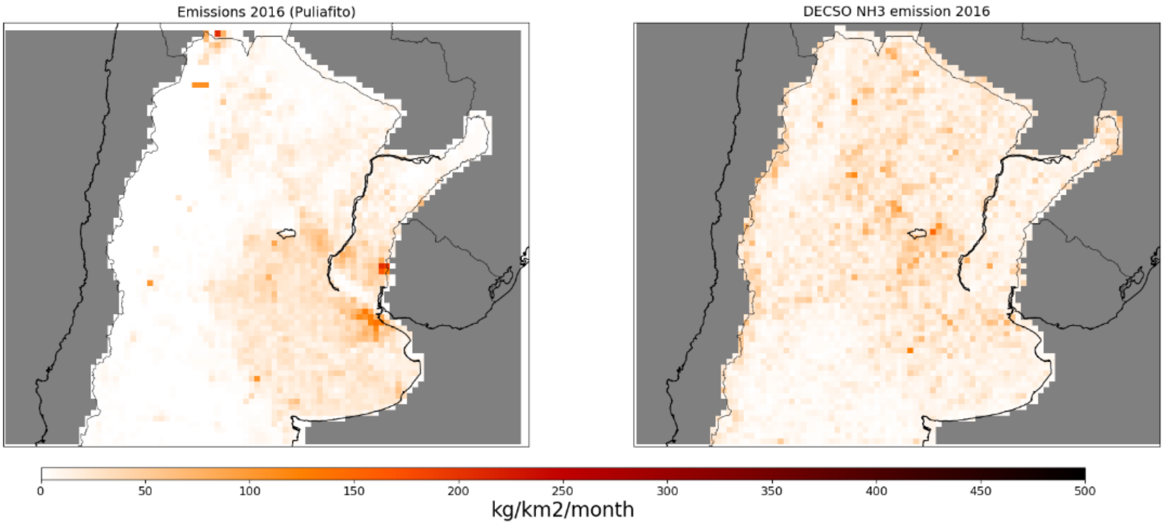

Figure 7 Comparison of the NH_3 emissions over Argentina from the bottom-up inventory in 2016 (left plot) and the DECSO emissions in 2016 (right plot).

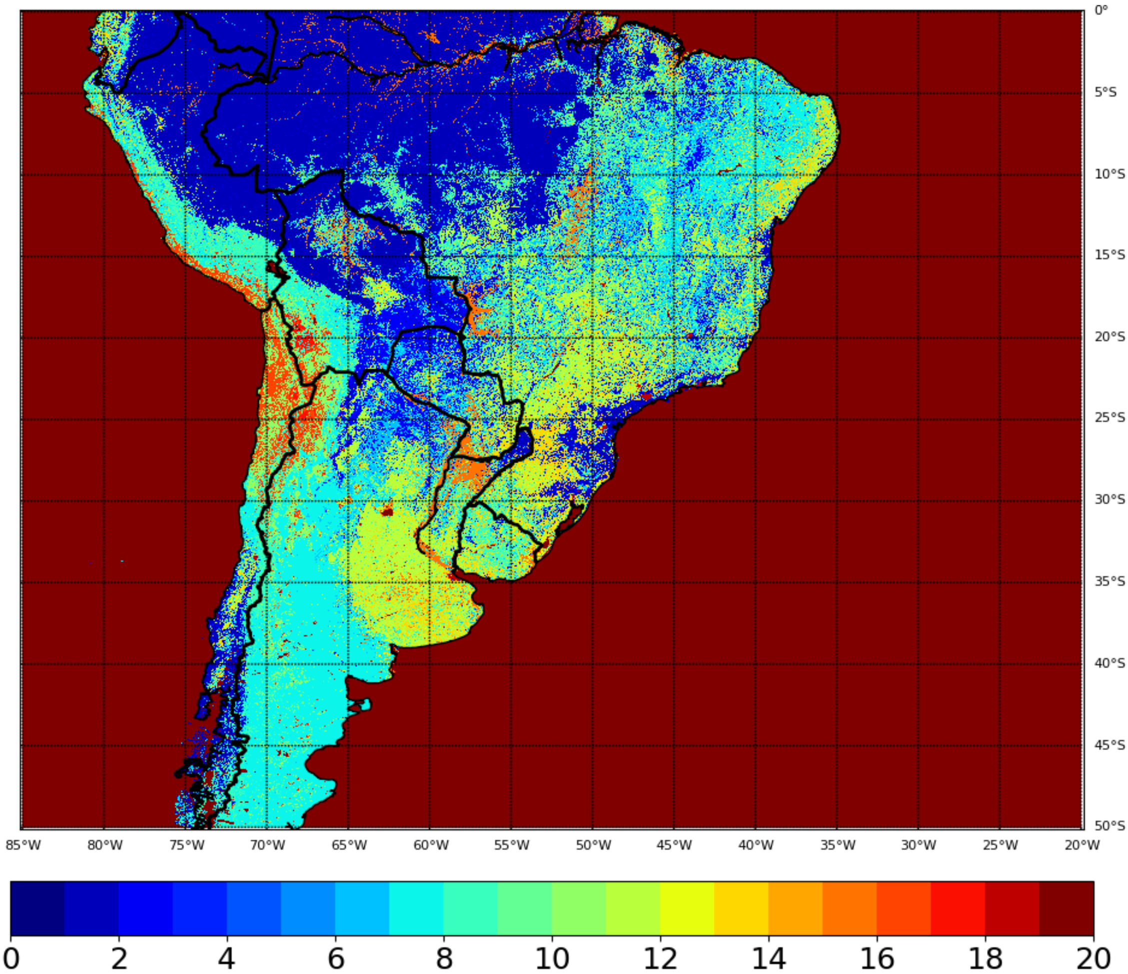

Figure 8. Landuse map in South America in 2013. The number represents different landuse categories. 1.Broadleaf Evergreen Forest; 2.Broadleaf Deciduous Forest; 3.Needleleaf Evergreen Forest; 4.Needleleaf Deciduous Forest; 5.Mixed Forest; 6.Tree Open; 7.Shrub; 8.Herbaceous; 9.Herbaceous with Sparse Tree/Shrub;

10.Sparse vegetation; 11.Cropland; 12.Paddy field; 13.Cropland / Other Vegetation Mosaic; 14.Mangrove; 15.Wetland; 16. Bare area, consolidated (gravel, rock); 17. Bare area, unconsolidated (sand); 18.Urban; 19. Snow / Ice; 20. Water bodies. The landuse dataset is the product version 3 from the Global Land Cover by National Mapping Organizations (GLCNMO). The data were prepared by using MODIS data with remote sensing technology. More information about the data can be found on https://globalmaps.github.io/glcnmo.html

Reference:
S. E. Puliafito, T. Bolaño-Ortiz, L. Berná, R. P. Flores, High resolution inventory of atmospheric emissions from livestock production, agriculture, and biomass burning sectors of Argentina, Atm. Environment, 223, 117248, doi:10.1016/j.atmosenv.2019.117248, 2020.

4 Publications related to DECSO

Ding, J., R.J. van der A, B. Mijling, P.F. Levelt and N. Hao, NOx emission estimates during the 2014 Youth Olympic Games in Nanjing, Atm. Chem. Phys., 2015, 15, 9399-9412, doi:10.5194/acp-15-9399-**2015**.

Ding, J., Miyazaki, K., van der A, R.J., Mijling, B., Kurokawa, J., Cho, S., Janssens-Maenhout, G., Zhang, Q., Liu, F., and Levelt, P.F., Intercomparison of NOx emission inventories over East Asia, Atm. Chem. Phys., **2017**, 17, 10125-10141, doi:doi.org/10.5194/acp-17-10125-2017.

Ding, J., R.J. van der A, B. Mijling and P.F. Levelt, Space-based NOx emission estimates over remote regions improved in DECSO, Atmospheric Measurement Techniques, **2017**, 10, 925-938, doi:10.5194/amt-10-925-2017.

Ding, J., van der A, R. J., Mijling, B., Jalkanen, J.-P., Johansson, L. and Levelt, P. F., Maritime NOx emissions over Chinese seas derived from satellite observations. Geophysical Research Letters, 45. https://doi.org/10.1002/2017GL076788, **2018.**

Mijling, B., R.J. van der A, K.F. Boersma, M. Van Roozendael, I. De Smedt and H.M. Kelder, *Reduction of NO2 detected from space during the 2008 Beijing Olympic Games*, Geophys. Res. Lett., **2009**, 36, doi:10.1029/2009GL038943.

Mijling, B. and R.J. van der A, Using daily satellite observations to estimate emissions of short-lived air pollutants on a mesoscopic scale. J. Geophys. Res. 117, D17, doi:10.1029/2012JD017817, **2012**.

Mijling, B., R.J. van der A and Q. Zhang, Regional nitrogen oxides emission trends in East Asia observed from space. Atmos. Chem. Phys., 13, 12003-12012, doi:10.5194/acp-13-12003-2013, **2013**.

van der A, R. J., Mijling, B., Ding, J., Koukouli, M. E., Liu, F., Li, Q., Mao, H., and Theys, N., Cleaning up the air: Effectiveness of air quality policy for SO2 and NOx emissions in China, Atm. Chem. Phys., **2017**, 17, 1775-1789, doi:10.5194/acp-17-1775-2017.

van der A, R.J., de Laat, A.T.J., Ding, J., Eskes, H.J., Connecting the dots: NOx emissions along a West Siberian natural gas pipeline, npj Clim Atmos Sci 3, 16, https://doi.org/10.1038/s41612-020-0119-z, **2020**.